atmosphere

MDPI

Article

Volcanic Glass as a Proxy for Paleotopography Suggests New Features in Late-Miocene Oregon

Julian Cohen *, John Bershaw and Richard Hugo

Department of Geology, Portland State University, Portland, OR 97201, USA; bershaw@pdx.edu (J.B.); hugo@pdx.edu (R.H.)

* Correspondence: jmcohen1721@gmail.com

Abstract: Volcanic glass has been used extensively as a paleoaltimeter. Deuterium (^{2}H) concentrations in glass have been found to be stable over geologic timescales, making δ^2H (also known as δD) a reliable proxy for ancient water chemistry. However, continued work revolves around better understanding how different factors affect preserved water in volcanic ash. Here, we analyze δD in the Rattlesnake Tuff (RST), a widespread ca. 7 Ma ash-flow tuff, and create a paleoisoscape to assess variations in δD across Oregon during that time. To this end, 16 ash samples were collected across central and eastern Oregon from various flow units within the RST. Samples were analyzed for δD using a temperature conversion elemental analyzer (TC/EA) connected to a mass spectrometer and elemental composition using a scanning electron microscope (SEM). We compared the isotopic results to modern water and published ancient water proxy data to better constrain changes in climate and topography across Oregon throughout the Neogene. We also estimated wt. % H_2O by calculating excess (non-stoichiometric) oxygen from SEM elemental data. We did not observe significant variations in δD among the flow units from single locations, nor was there a significant relationship between the prepared glass shard composition and wt. % H_2O or δD, supporting the use of volcanic glass as a reliable paleoenvironmental indicator. Our results show significant spatial variation in δD_{water} values of RST, ranging from −107‰ to −154‰. δD values of ancient glass were similar to modern water near the Cascade Mountains but became relatively negative to the east near the inferred eruptive center of the RST, suggesting that a significant topographic feature existed in the vicinity of the RST eruptive center that has since subsided.

Keywords: volcanic glass; paleotopography; stable isotopes

Citation: Cohen, J.; Bershaw, J.; Hugo, R. Volcanic Glass as a Proxy for Paleotopography Suggests New Features in Late-Miocene Oregon. *Atmosphere* **2024**, *15*, 561. https://doi.org/10.3390/atmos15050561

Academic Editor: Yougui Song

Received: 29 December 2023
Revised: 9 April 2024
Accepted: 22 April 2024
Published: 30 April 2024

1. Introduction

The stable isotopic composition of environmental water is highly reliant on topography, climate, and geographic location. Therefore, reconstructing ancient water isotopes from the rock record is one way to constrain how a landscape has changed over time. Hydrogen isotopes preserved in vitreous volcanic glass have been established as a useful proxy for understanding paleoprecipitation and paleoenvironments ([1–5]). The utility of volcanic glass as a paleoenvironmental proxy is two-fold. First, volcanic glass is known to quickly (within 10 ka of deposition) incorporate environmental water and preserve its H isotope composition over geologically significant timescales [4,6–8]. Second, minerals within volcanic glass are easily dated radiometrically, giving interpretations a reliable temporal context.

Since the beginning of the Cenozoic, the Pacific Northwest has evolved topographically, undoubtedly responsible for changes in regional climate [9–11]. Previous work has aimed to better understand these changes using δD from volcanic glass and other paleoenvironmental proxies, though there are varied interpretations about their timing and spatial extent [4,11–14].

This paper focuses on the topographic evolution of the area to the east of the Cascades, which has previously not been studied in detail. We constrain how stable hydrogen isotopic compositions derived from the Rattlesnake Tuff (RST) vary regionally to better understand the controls on this paleoclimate proxy as well as constrain the paleoclimate of central Oregon during the Miocene.

The RST exists today as a widespread, mostly flat-lying ash-flow tuff. There is little variation in unit thickness, with beds thickening slightly toward the inferred eruptive center [15]. There are no known outcrops of the RST immediately around the eruptive center (Figure 1) because it is overlain by younger basalt deposits [16]. Today's flat-lying, horizontally continuous RST outcrops suggest that the landscape in areas currently covered with RST were flat-lying ca. 7 Ma [17]. Despite appearing on ridgetops and valley floors, thickness variations in RST outcrops are quite small (tens of meters) [15]. The low aspect ratio (average thickness/distance) of ~10^{-4} (cf. Figure 2 from [18]) of the RST indicates a high-energy ash-flow depositional environment. The flat-lying nature of RST outcrops suggests that any topographic features associated with High Lava Plains' volcanism in or near Harney Basin were localized. During the late Miocene, the Harney Basin and surrounding areas were volcanically active, with many silicic domes and ash-flow tuffs erupting from the region during that time [17,19,20].

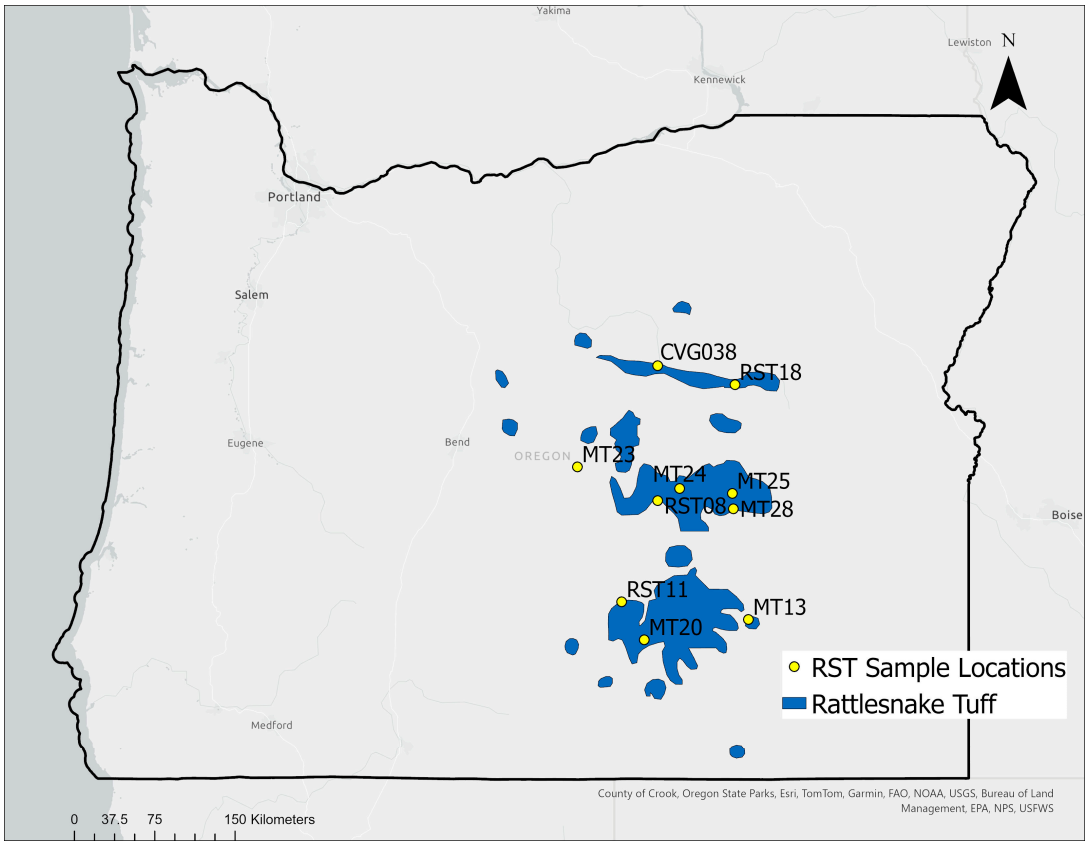

Figure 1. Map showing the spatial extent of the Rattlesnake Tuff in blue. Samples analyzed for this work are shown with yellow dots. Adapted from Streck and Grunder [15]. Samples RST08, RST11, and RST18 were collected in 2018. Sample CVG038 was published in Bershaw et al. [4].

We sampled the Rattlesnake Tuff, a spatially extensive Miocene rhyolitic ash-flow tuff ([15]; Figure 1), and collected two datasets: (1) δD values for 17 samples (16 from this study and 1 from Bershaw et al. [4], described in Table S1), producing a "paleoisoscape" (e.g., [21]) that was compared to spatial patterns in modern water δD, and (2) SEM major and minor element data to better understand compositional and textural controls on variations in δD among tuff samples. With this information, we answer the following questions: How do

δD values from the Rattlesnake Tuff compare to δD values derived from modern water? How and why do isotopes in the widespread Rattlesnake Tuff vary spatially across eastern Oregon? How can differences between modern and ancient isotope records be explained through changes in climate and topography? Are any of the observed variations in δD able to be explained through changes in glass texture or composition?

2. Materials and Methods

2.1. Sample Collection

Samples were collected from various outcrops located in central and eastern Oregon during August 2022 (Figure 1). Sites were selected if their descriptions indicated non-welded to moderately welded tuffs. Tuff samples were non-welded to partially welded, with abundant glass and low degrees of secondary low-temperature mineralization and oxidation on the surface of glassy shards. All samples contained abundant glassy shards. Samples were collected from the non-welded basal portion of the outcrop. In 2 localities, the incipiently welded ash fall layer was sampled. These are indicated in Table S1. Outcrop locations were selected based on mapping from Streck and Grunder [15] and were chosen based on descriptions describing the presence of non-welded to moderately welded portions of the RST. Another characteristic feature of the RST that helped in identifying outcrops is the presence of compositionally distinct pumice clusters [22]. Due to the importance of selecting samples of the same age, selected outcrops were carefully adhered to. Approximately 1 kg of sample was collected from 10 to 30 cm into the outcrop surface to reduce the influence of weathering and oxidation. This improved the chance that samples contained pristine glass, and that there was enough material to be properly processed.

2.2. Sample Preparation

For mass spectrometer analysis, the sample preparation methods employed are outlined by Cassel and Breecker [8], and we used hydrofluoric acid (HF) treatment to effectively remove surface contaminants [23]. Samples were crushed with a ceramic mortar and pestle. The crushed samples were wet-sieved using nylon screens with 150 and 70 μm filters. The filtered 70–150 μm fraction of glass shards was washed two to three times in 10% hydrochloric acid (HCl) for 30 s to remove carbonates. Samples were then washed one to two times in 8% HF for 30 s. This removed contaminants still bonded to the surface as well as the outermost layer of potentially altered glass. Magnetic minerals were removed with a hand magnet. Samples were further sorted through gravity separation using the heavy liquid lithium metatungstate (LMT) diluted to 2.7 g/cm^3 to match the desired density of "pure" glass shards.

A small block (1 × 3 cm) was cut and impregnated with epoxy. After at least 24 h of curing, the sample was polished to a microprobe-quality finish (0.3 μm grit) for SEM-energy dispersive X-ray spectroscopy (EDS) elemental analysis. Samples were examined in a Zeiss Sigma-VP FEG-SEM at 11 nA. X-ray elemental analysis was performed with an Oxford Aztec 6.0 system with an UltimMax 65 EDS detector. These instruments were manufactured by Oxford Instruments, plc, Abingdon, UK.

2.3. TC/EA Sample Analysis

A total of 16 samples were analyzed using the TC/EA high-temperature conversion elemental analyzer (TC/EA) isotope ratio mass spectrometer at the University of Texas Austin's Light Stable Isotope Laboratory. Each sample and standard were weighed into three ~6 mg silver foil capsules for analysis. All samples and standards were run in triplicate to ensure measurements were unaffected by previous analyses. The results are reported as δD_{glass} and were converted to δD_{water} using the following equation from Friedman et al. (1993) [7].

$$\delta D_{water} = ((1000 + \delta D_{glass})/0.967) - 1000 \quad (1)$$

This conversion allows for a direct comparison between ancient δD values derived from glass analyses and δD values obtained from modern water samples.

Isotope Data and Interpolation

Isoscapes were generated using interpolation tools in ArcGIS Pro. ArcGIS Pro is produced by Environmental Systems Research Institute, Inc., Redlands, CA, USA. The modern isoscape (Figure 2) was created by Bowen [24] based on the methodology from Bowen and Revenaugh (2003). The data that informed this model are from the Global Network of Isotopes in Precipitation [25] and Welker [26]. For the RST isoscape, the Natural Neighbors interpolation tool was used. This dataset was challenging to represent well with interpolation due to its distribution (not normal) and a small number of control points. The Natural Neighbors tool was selected because it works well for small datasets.

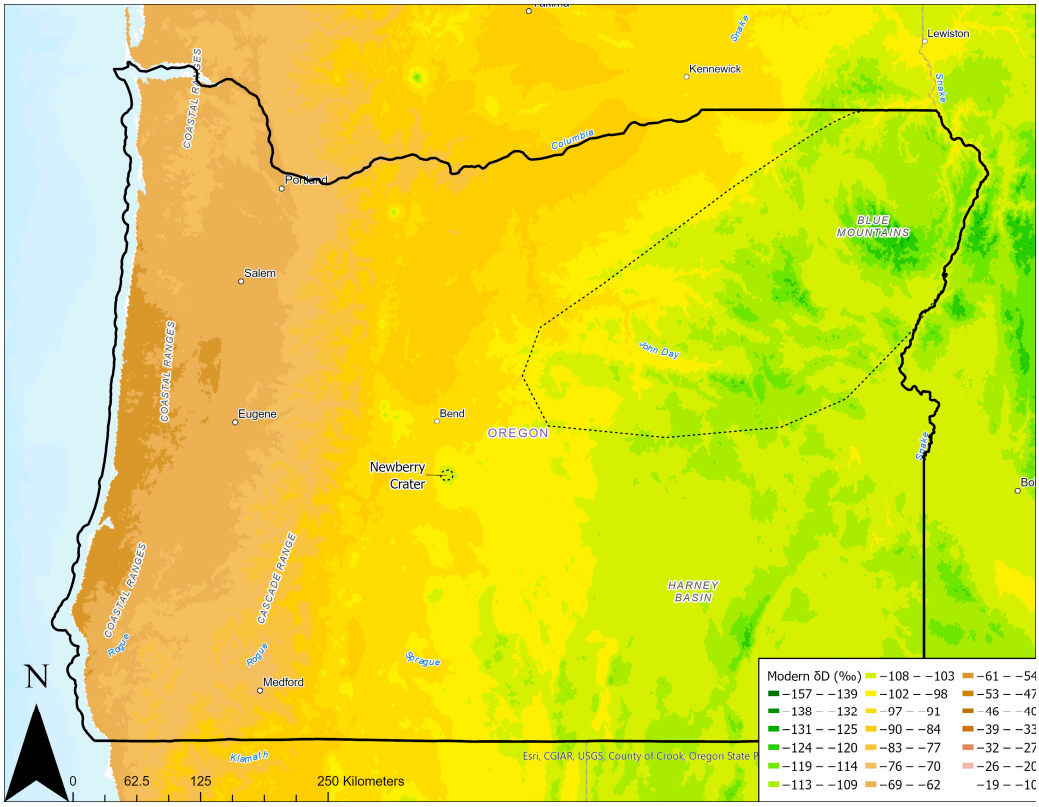

Figure 2. Isoscape showing modern mean annual δD in precipitation. Gridded map data are from Bowen, G.J. [24]. The interpolation methodology is from Bowen and Revenaugh [27]. Data are from GNIP [25] and Welker [26]. The dashed area encompasses the Blue Mountains and Newberry Crater.

2.4. SEM Sample Analysis

We analyzed compositional variations in a glass sample (MT-23) with a distinct oxidation rim and unoxidized interior to determine whether weathering processes affect the wt. % water of glass. The sample was chosen because it had visible, pristine, vitric shards in its interior with a pronounced weathering rind. These features made it easy to compare oxidized and unoxidized glass. Volcanic glass can undergo a variety of weathering and alteration processes such as devitrification, leaching, and secondary mineralization, all of which have the potential to overprint paleoclimate signatures. Because of this, a rigorous methodology for selecting "pristine" glass shards was used [8]. While past studies have suggested that this procedure is effective for isolating unaltered glass [4,8,23], scanning electron microscope imaging was used to verify observations from the petrographic microscope. In this study, we used the SEM to gather both chemical and textural data of glasses that exhibit secondary mineralization on their surface and those that do not so as

to independently determine their suitability for analysis. These analyses were performed before sample preparation for isotopic analysis.

2.5. Effect of Oxidation and Surface Mineralization on Water Content in Untreated Tuff

We utilized a backscattered electron detector (BSD) and energy-dispersive X-ray (EDX) spectrometer manufactured by Oxford Instruments plc, Abingdon, UK, to collect average Z and chemical data. Using the BSD detector, we imaged both oxidized and unoxidized sections of the sample and compared them, looking specifically for shards that have distinct internal variations in BSD grayscale brightness (Figure 3). Sections were predetermined to be oxidized or unoxidized based on visible discoloration of the sample. Once these were found, we used the EDX detector to gather chemical data in areas with notable BSD contrast (Figure 3). We chose to analyze only moderately weathered glass, as more weathered samples are not suitable for isotope analysis.

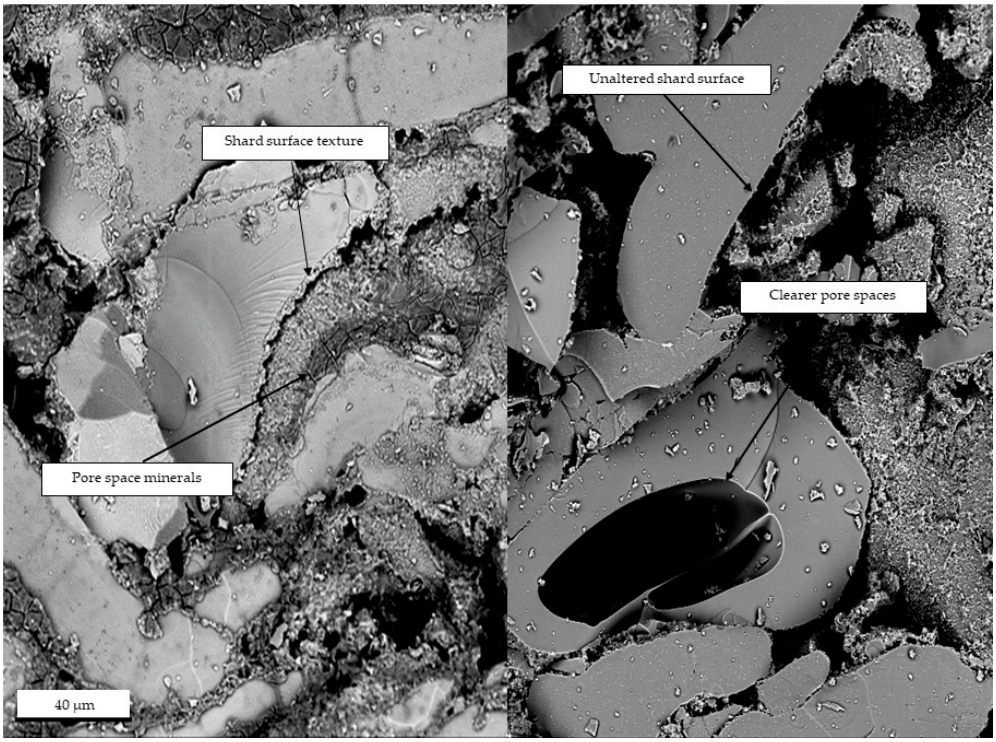

Figure 3. Backscattered electron images of sample MT-13c. The left image was taken within the oxidation rind to show secondary mineralization textures in pore spaces and on shard surfaces. The right image shows fewer secondary minerals forming outside of the oxidation rind. The scale is the same for both images.

2.6. SEM Data Analysis

Effect of Oxidation and Surface Mineralization on Water Content in Untreated Tuff

We obtained 69 individual measurements across 6 different sites in the oxidized and unoxidized sections of the sample (Table S2). Data were accepted if their non-normalized totals of major element compositions were between 90% and 105%. The results were normalized to 100% total and exported as tables, with totals calculated both with the "All Elements" and "O by Stoichiometry" settings in Aztec (Supplementary Materials). With these data, we employed methods from Kotov et al. [28]. They show that SEM energy-dispersive spectrometry (EDX) can be effectively employed to assess the water content of high silica glasses [28]. This method is effective in glasses with at least 0.5 wt. % H_2O. Excess oxygen was calculated using Equation (2):

$$C_{H_2O} = 1.126\left(C_O - \sum C_i \frac{V_i A_O}{2A_i}\right) \quad (2)$$

where C_O and A_O are the concentration and atomic weight of oxygen, and C_i, A_i, and V_i are the concentration, atomic weight, and valence of element i [28]. The result, if positive, reflects that some oxygen is bonded to hydrogen, which is undetectable with EDX. We assume that this excess oxygen is representative of water in the sample. The means were compared using a two-mean t-test to assess for similarities in the populations (Figure 4).

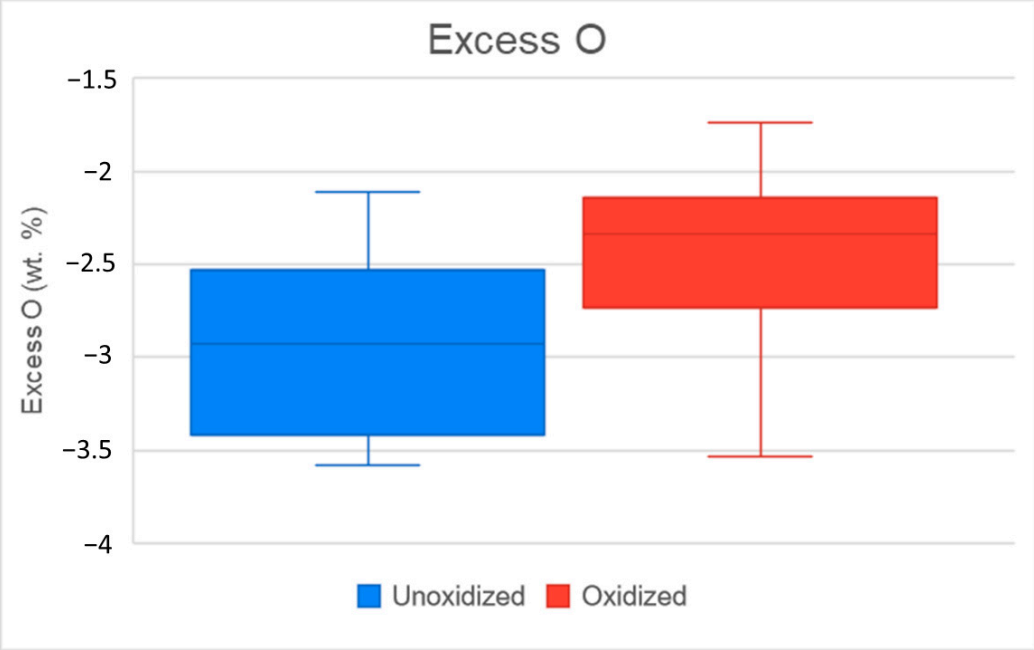

Figure 4. Box-and-whisker plot showing distributions of excess O in both oxidized and unoxidized datasets. Two-mean t-test provides p-values of 0.3452 suggesting there is no significant difference between the mean excess O values.

3. Results

3.1. SEM Results

The oxidized tuff has a mean excess O of −3.88 and a mean grayscale of 89.22, while the unoxidized tuff has a mean excess O of −2.62 and a mean grayscale of 83.74. This suggests that the water content is approximately equal despite qualitative compositional differences. The two-mean t-test shows that there is no significant difference in excess O between the oxidized and unoxidized datasets (Figure 4).

3.2. TC/EA Results

δD values are highly varied, with δD_{glass} values ranging from −182‰ to −137‰. The water content of the glasses ranges from 2.7 to 5.1 wt. % H_2O. Carlson [23] reports an average wt. % H_2O of 2.95 for the Rattlesnake Tuff across two samples, within the range of new data presented here. We present one δD value (CVG038) from Carlson [23] and omit CVG039 because we analyzed a sample from the same outcrop and present its δD value.

Samples MT-28d and MT-28dm, as well as samples MT-28b and MT-28bm, have nearly identical δD values despite being nonmagnetic and magnetic, respectively (Table 1). This is expected as they are from the same sample. Thus, the presence of magnetic elements in the glass (Fe, Mg) does not appear to impact isotopic composition. The isoscape (Figure 5) was generated to show how δD values are distributed spatially. The modern δD record shows deuterium depletion (decreasing) toward the northeast, with relatively positive δD values in the southwest. In the ancient record, the lowest δD values are concentrated in the center of the study area, notably close to the inferred eruptive center of the Rattlesnake Tuff from Streck and Grunder [22].

Table 1. Isotopic results for RST samples presented in this study. Sample CVG038 is from Bershaw et al. [4]. Samples beginning with "RST" were collected by others in 2018 but prepared and analyzed as part of this research. Sample MT-14b (starred) is interpreted to be an older non-welded tuff known as the Devine Canyon Tuff (9.7 Ma). The 1σ analytical uncertainty for δD is ±1‰. * Sample MT-14b was later determined to be part of the differently-aged Dinner Creek Tuff. It was not included in spatial isotope analysis.

Sample	δD_{glass}	δD_{Water}	Wt. % H_2O	Depositional Environment	Hydration Water	Latitude	Longitude
MT-13c	−169	−140	5.1	Ash Fall	Precipitation, Fluvial	42.9839	−118.8731
MT-14b *	−166	−138	2.9	Ash Flow	Precipitation, Fluvial	43.0258	−118.63633
MT-19	−140	−111	3.4	Ash Flow	Precipitation, Fluvial	42.8404	−119.66862
MT-20	−151	−122	2.9	Ash Flow	Precipitation, Fluvial	42.8596	−119.74695
MT-21	−137	−107	3.1	Ash Flow	Precipitation, Fluvial	42.7868	−120.2242
MT-23	−149	−120	2.9	Ash Flow	Precipitation, Fluvial	43.9135	−120.30725
MT-24b	−175	−147	3	Ash Flow	Precipitation, Fluvial	43.7829	−119.45026
MT-25	−147	−118	2.8	Ash Flow	Precipitation, Fluvial	43.7525	−119.00905
MT-28a	−178	−150	3.2	Ash Fall	Precipitation, Fluvial	43.6593	−118.99916
MT-28b	−182	−154	2.8	Ash Flow	Precipitation, Fluvial	43.6593	−118.99916
MT-28bm	−182	−154	2.7	Ash Flow	Precipitation, Fluvial	43.6593	−118.99916
MT-28d	−181	−153	2.7	Ash Flow	Precipitation, Fluvial	43.6593	−118.99916
MT-28dm	−181	−153	2.7	Ash Flow	Precipitation, Fluvial	43.6593	−118.99916
RST2018_08	−173	−145	2.9	Ash Flow	Precipitation, Fluvial	43.7096	−119.6356
RST2018_11	−156	−128	2.7	Ash Flow	Precipitation, Fluvial	43.0922	−119.93541
RST2018_18	−158	−129	3.9	Ash Flow	Precipitation, Fluvial	44.4082	−118.98748
M2-CVG038	−146	−117	2.9	Ash flow	Precipitation, Fluvial	44.5212	−119.63343

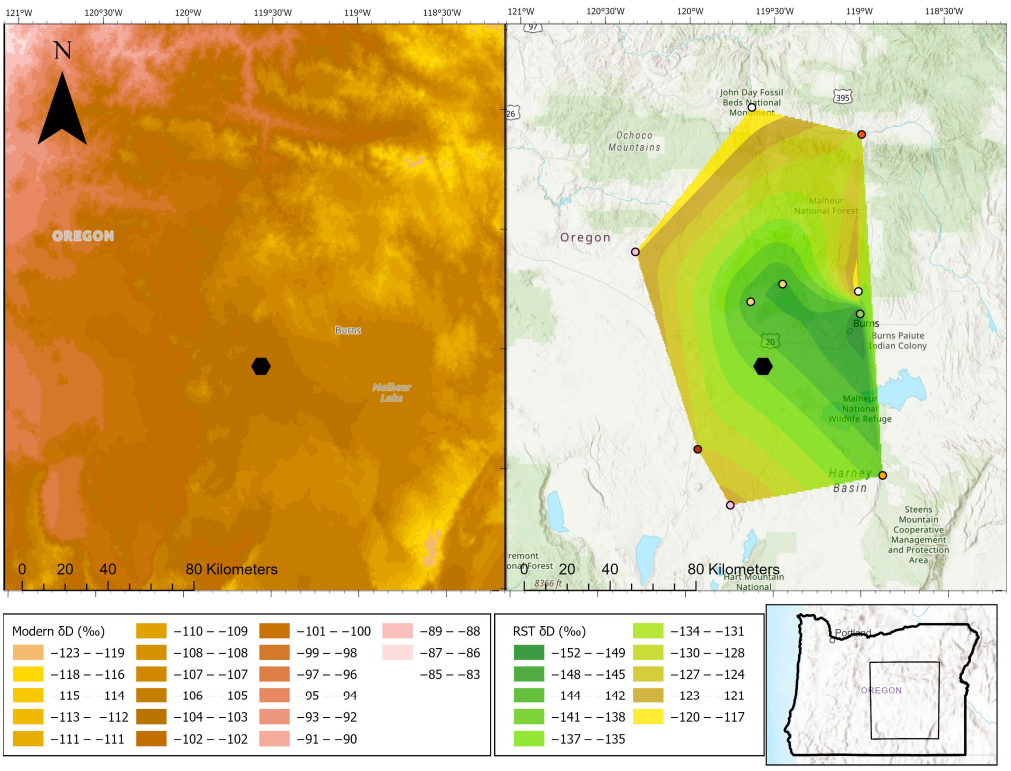

Figure 5. Isoscapes showing δD variation across the study area ca. 7 Ma and today. The inferred eruptive center is shown with the black hexagon. Latitude is shown along the top of the map area. Black dashed horizontal lines divide the map into "low", "middle", and "high" latitudes. Interpolation control points use the same color scale.

There are significantly different patterns between modern and ancient δD values when comparing longitudinal trends (Figure 6). Eastward, deuterium depletion in 7 Ma volcanic glass occurs at nearly four times the rate in the modern system. The results also show no significant relationship between ancient δD and modern elevation (R^2 = 0.09), while we do observe a weak relationship between modern δD and modern elevation (R^2 = 0.34), typical of rain shadows elsewhere (Figure 2) [29].

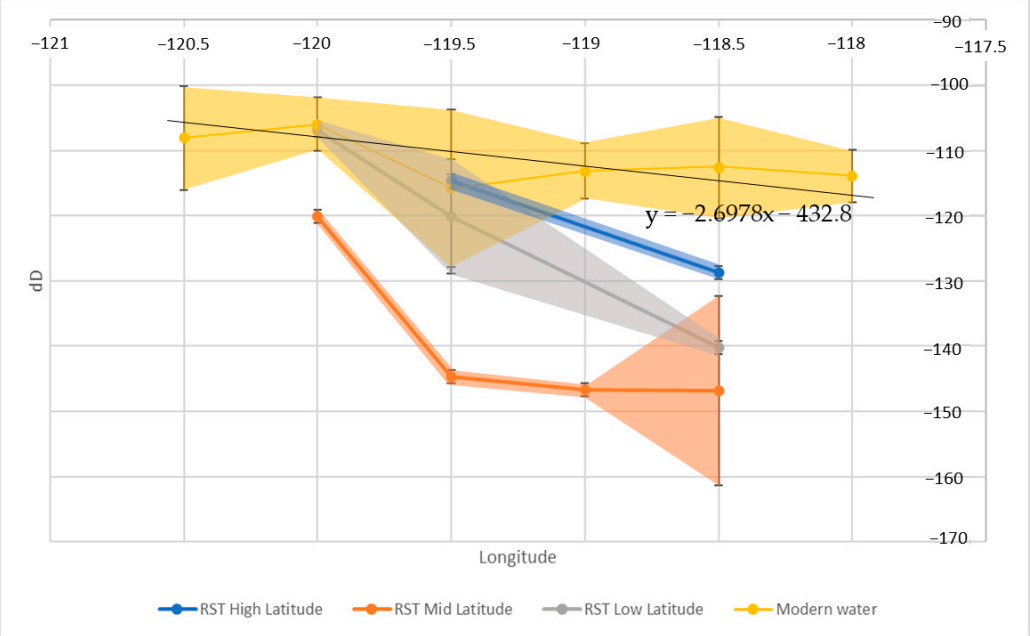

Figure 6. Scatterplot bins average δD every 0.5 degrees longitude. Error bars represent the uncertainty of averaged δD values. δD values for RST were converted to δD_{water} using the Friedman [7] equation. Significant δD depletion at id-latitude ca. 7 Ma is interpreted to reflect paleotopography. Low, mid, and high latitudes are defined in Figure 5. The trendline represents the equation used to correct for the continental effect.

4. Discussion

4.1. Effects of Oxidation and Surface Mineralization on the Passivating Layer

Though brightness variations in backscattered images suggested the possibility of chemical variation within different glass regions, our data do not support this hypothesis. In particular, our data support the finding that excess O, and by extension water, is approximately equally abundant in both tuff populations. A *t*-test statistic of 0.3452 confirms that there is no significant difference between the excess O in the oxidized and unoxidized sections of the sample. Therefore, we conclude that while compositional differences exist between oxidized and unoxidized tuff, it is not a result of differences in water content. This finding confirms that glass that is suitable by optical standards is also suitable for isotopic analysis, regardless of potential compositional differences.

4.2. Effect of Magmatic Water on Volcanic Glass δD

Magmatic δD values are typically much less depleted in deuterium relative to those measured (roughly −40‰–−80‰) [30,31]. Therefore, δD values measured closer to the inferred eruptive center would likely show higher (less negative) δD values, as glasses in thicker cooling units have the potential to be rehydrated by degassed magmatic water sourced from deeper in the unit [30]. In addition, we analyzed glass shards at the size fraction (70–150 μm), which have been shown to hydrate completely based on diffusion modeling [8]. Our results suggest that magmatic water does not influence our δD values as they are relatively depleted around the inferred eruptive center of the RST (Figure 5).

Highly explosive eruptions such as the RST have been shown to retain between 0.2 and 0.6 wt. % magmatic water, suggesting that well-hydrated glasses such as those in this study are dominated by meteoric water [30,32]. Additionally, a significant relationship between δD and wt. % H_2O is commonly viewed as a metric for magmatic water influence. In our results, there is no statistically significant relationship between these variables (R^2 = 0.007), indicating that magmatic water does not influence the measured δD values.

4.3. Paleoenvironmental Interpretations

The lack of a meaningful correlation (R^2 = 0.09) between modern elevation and δD values measured from ancient (7 Ma) glass strengthens the assumption that well-prepared volcanic glass produces δD values that reflect ancient meteoric water and that topography and/or climate was different in the late Miocene relative to today. Furthermore, spatial trends in the modern isoscape have very different magnitudes from those in the ancient isoscape ~7 Ma (Figure 5).

The framework used in this paper for interpreting spatial patterns in stable isotopes is based on models of meteoric water isotope evolution from previous workers [33,34]. The continental, amount, and altitude effects describe the tendency for stable isotopes in meteoric water to fluctuate in response to changes in environmental conditions (distance from the ocean, amount of precipitation, and elevation). While modern and ancient water δD values both decrease to the east, the magnitude of depletion in ancient samples is much higher. Over the same distance from west–east (approximately 200 km), δD decreases nearly four times more in the ancient system as compared to the modern system (Figures 6 and 7). The marked decrease in δD is centered around a relatively small area, which is inconsistent with changes in regional climate due to the continental or amount effects, as these factors would affect the isotopic composition of ancient meteoric water over much larger areas [34].

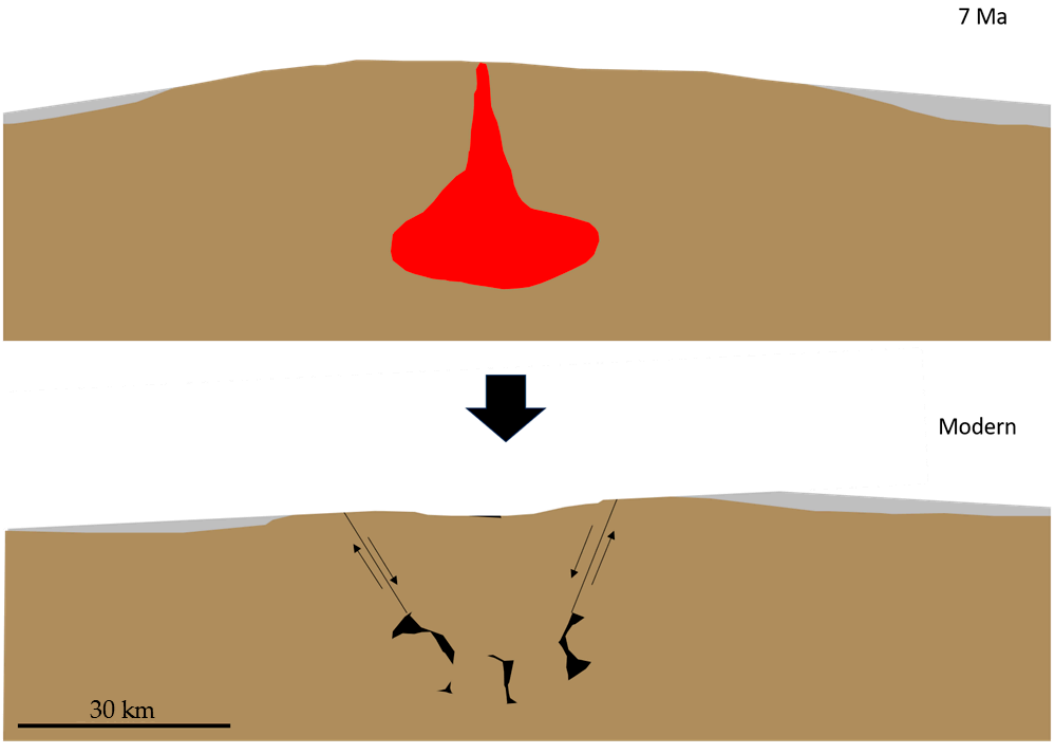

Figure 7. Simplified cross-section of an isolated topographic feature that may explain the observed depletion in δD of ~7Ma hydrated volcanic ash. A large magma chamber would have supported a large volcanic edifice or dome. Following the rapid evacuation of the magma chamber, the volcanic edifice would have collapsed (structurally or due to changes in isostasy). Regional subsidence from the cooling of the lithosphere may have resulted in the lowering of remaining RST outcrops to elevations seen today.

The difference in the modern and 7 Ma isoscape is not likely due to changes in Cascade elevation given that east of the range at approximately −120° longitude, modern and ancient δD values are nearly identical (Figure 6). We interpret this to suggest that the Cascades and other topographic features to the west (the Oregon Coast Range) were likely significant topographic features in the late Miocene (~Ma).

In modern central Oregon, the altitude effect accounts for a significant portion of the localized variation in δD (R^2 = 0.34). Areas such as the Blue Mountains in northeastern Oregon and other isolated peaks feature localized depletions in δD associated with increases in elevation (Figure 2). δD values derived from the RST present a similar local pattern of more negative δD centered north–northeast of the Harney Basin, which is its inferred eruptive center [17] (Figure 5). Accordingly, the pattern seen in Figure 5 is consistent with δD depletion due to an isolated topographic high, such as a volcanic dome.

4.3.1. Lapse Rates and Elevation Estimates

Given that the lowest δD values in the paleoisoscape are concentrated around the eruptive center inferred by [22], we propose that the region that is now located near Burns, OR, west–northwest of the Harney Basin, contained a significant topographic feature ~7 Ma. This interpretation is consistent with the trends observed in modern meteoric water (Figure 2), where the Blue Mountains in NE Oregon and peaks around Newberry Crater in central Oregon cause localized decreases in meteoric water δD. The difference in elevation between Bend, Oregon and the summit of Newberry Crater is approximately 900 m (Figure 2). The associated change in δD is ~−11‰ (−110‰ in Bend and −121‰ at Newberry Crater) [35] or −12.2‰/km. An isotopic lapse rate for the Ochoco Mountains to the northwest of the study area has been established for δD of −16.8‰/km of elevation gain [36] based on a weighted average of high- and low-elevation precipitation stations on the windward side of the range. This isotopic lapse rate is steeper than that observed on the western side of the Cascades, which is −20.6‰/km [37]. We estimated the paleoelevation of a volcanic dome that sourced the RST in the modern Harney Basin based on modern lapse rates (−20.6‰/km and −12.2‰/km) and observed a decrease in volcanic glass δD of −35‰ ~7 Ma.

To calculate paleoelevation, we first corrected our data for the continental effect by calculating a linear fit through the modern δD data (Figure 6). This equation represents the rate of change in δD associated with changes in longitude in modern central and eastern Oregon. By fitting this line and subtracting it from our RST δD values, we determined the change in δD associated only with changes in elevation. Next, we calculated the magnitude of the change in δD associated with paleotopography by subtracting the average RST δD value at −120° longitude from the average RST δD value at −118.5° longitude. The result including the error shown in Figure 6 is between −14.6257‰ and −42.6257‰ over the observed range in longitude. We applied the previously discussed lapse rates to these changes to estimate paleoelevation with relief between 700 m and 3.5 km.

Atmospheric pCO_2 has been shown to impact isotopic lapse rates [38]. Atmospheric pCO_2 ca. 7 Ma was higher than today due to higher global temperatures, which may have resulted in lower isotopic lapse rates generally. This suggests that our paleoelevation estimate is conservative.

Previous work by Galewsky [39] aimed to describe the effects of atmospheric stratification, relief, wind speed, and horizontal aspect ratio (β) of topography on isotope ratios in precipitation. Particularly high topography can cause air parcels to stagnate, reverse direction, or flow around the feature, complicating the use of the altitude effect alone to interpret paleoelevation proxies [39]. Such phenomena have been shown to significantly alter the isotopic lapse rate. The topographic feature we propose is comparable to modern eruptive centers with large, broad topographic features (β = 1). The island of Hawaii, which may have a similar aspect ratio to the proposed RST feature, has a smaller isotopic lapse rate than would be predicted by traditional Rayleigh distillation models [39]. This phenomenon is explained by the flow of air parcels around the topographic feature, with

less air flowing over the top of the feature. Tachera et al. [40] report isotopic lapse rates for Hawaii similar to those we present in this paper (−13.6‰/km for low–mid elevations and −24‰/km for higher elevations). That said, the extent to which stratified atmospheric flow over and around topography with a circular footprint affects orographic precipitation isotopic ratios is unknown [39].

Overall, our results point toward a prominent, isolated topographic feature with relief of 700 m–3.5 km near the inferred eruptive center of the RST. This large range accounts for varying lapse rates in modern eastern Oregon and captures the uncertainty related to the effects of differing atmospheric conditions resulting from global climate change, atmospheric flow dynamics around isolated topography, and longitudinally binned means.

4.3.2. RST Stratigraphy and Paleotopography

It seems plausible that significant topographic features could have existed in eastern Oregon during the late Miocene. Kukla et al. [41] describe similar isotopic patterns in the Blue Mountains, suggesting that changes in elevation and precipitation seasonality throughout central Oregon have contributed to isotopic trends throughout the Cenozoic.

There are also features in outcrops around the inferred eruptive center that support this interpretation. First, RST outcrops are thickest ~30–40 km from the inferred eruptive center, and thin both toward and away from these thickest areas [15]. Thinning toward the eruptive center is consistent with the deposition on the flanks of a topographic feature. This can be explained by topography (Figure 7).

In addition to topography, samples with the lowest δD may have been located in the lee of the RST topographic feature. If this were the case, the lowest RST δD values would represent a combination of elevation and rainout of heavier isotopes over the highest parts of the topographic feature. Our estimations of paleotopography are based on RST δD values in the mid-latitude portion of the study area. While this region showed the steepest and most extreme lapse rates, areas north and south of the eruptive center also showed steeper and more extreme changes in δD compared to modern values. Higher lapse rates north and south of the eruptive center suggest that topography associated with the RST eruptive center may have been quite broad (Figure 7). Uplift caused by regional heating from the large magma chamber could have caused uplift of this spatial scale.

Prior to the eruption of the RST (~8 Ma), regional volcanic activity had produced voluminous flood basalts in areas to the north and south of the RST eruptive center [16].

Notably, outcrops of these basalts within the area of the RST eruptive center have not been reported in the published literature. The presence of significant topography associated with the RST eruptive center could explain the absence of 7.1–8 Ma basalt outcrops in this area. Overlying the RST eruptive center today are younger ferro-trachytic basalts aging 5.4–2.2 Ma [16], which are compositionally distinct from basalts from the 8 Ma and are thought to have been emplaced during a period of thermal subsidence. A gap in flood basalt emplacement between 8 and 5.4 Ma in the geographic region of the RST eruptive center suggests topography could have existed for at least 2.6 million years. Spatial variations in the thickness of these basalt flows are not well documented in the published literature, making it difficult to interpret changes in flow thickness in response to deposition on or around topographic features. This is likely due to limited exposures of these units, which are found in canyons and along fault scarps [42].

The High Lava Plains province is an area characterized by abundant basalts, andesites, rhyolites, and other intermediate lavas [16,42–44]. In the period immediately prior to the eruption of the RST (8–7.1 Ma), significant volumes of flood basalts were erupted and emplaced in areas north and south of the RST eruptive center. These eruptions, which culminated with the emplacement of the RST at 7.1 Ma, were accompanied by significant regional warming. The magmatic warming of the crust may have resulted in regional uplift near the RST eruptive center, causing flood basalt emplacement to occur at the margins of higher topography.

The basaltic magmas from this pre-RST episode erupted through dikes associated with the Brothers Fault Zone (BFZ) [43,44]. This represents a regional transition from extensional accommodation by Basin and Range normal faulting to extensional shearing in the BFZ [44]. Regional subsidence is likely to have lessened with this transition and could have contributed to the uplift of significant topography.

Overall, the spatial distribution of pre- and post-RST flood basalt outcrops supports the existence of high topography in the geographic region around the RST eruptive center for at least 2.6 million years. This topography would have been the result of regional warming for ~900 thousand years prior to the RST eruption and a transition from extensional Basin and Range normal faulting to BFZ shearing.

4.3.3. Modern Analogs

There have been few eruptions like the RST in recent times. However, the Novarupta-Katmai eruption in Alaska in 1912 has many similarities to the RST. The eruption took place over ~60 h and expelled 13–14 km^3 of magma from a zoned chamber [45]. It is a part of the volcanically active Valley of Ten-Thousand Smokes (VTTS) region, which features many volcanic edifices of varying heights, ranging from 65 m (the product of the Novarupta eruption) to 2330 m [45]. The VTTS is similar to the HLP in that it lies in a back-arc setting. This shows that volcanically active regions that produce large, voluminous rhyolitic eruptions do create significant topographic features, as the RST likely did in central Oregon ~7 Ma ago.

The Chaitén Volcano in Chile is an additional modern analog for caldera-producing rhyolitic eruptions. The last major eruption of Chaitén was ~10,000 years ago, which resulted in a caldera collapse and subsequent effusive construction of a large lava dome ~400 m high [46]. The dome is estimated to be ~5600 years old and is part of a feature with a total relief of ~850 m. Notably, both of these topography-forming volcanic centers are orders of magnitude smaller than the RST in terms of total erupted volume. We propose the RST feature to be broader and higher, with topography likely a function of regional heating by mantle processes active in the region ca. 7 Ma (e.g., [42,43]). The high, broad dome feature we propose fits the relative magnitude of the RST eruption.

5. Conclusions

We presented new stable isotopic and compositional data for 16 glass samples collected from the Rattlesnake Tuff in central Oregon. With these data, we showed that δD values derived from the ~7 Ma RST exhibited anomalously low δD values clustered near their inferred eruptive center. We also showed that there were no significant variations in δD within outcrops. We showed that compositional variation among glass shards was not associated with differences in wt. % H_2O or δD. We also showed that there was no statistically significant relationship between wt. % H_2O and δD, suggesting that the magmatic signal had a negligible effect on hydrated glass δD values. Overall, we conclude that relatively low δD values centered near the inferred RST eruptive center may be explained by an isolated topographic feature within the present-day Harney Basin, likely related to the eruption of the RST. Using three different modern δD lapse rates, we estimated the paleoelevation of the ~7 Ma RST volcanic feature to have been 700 m–3.5 km above the surrounding region to account for the observed decrease in ancient water δD.

Supplementary Materials: The following supporting information can be downloaded at: https://www.mdpi.com/article/10.3390/atmos15050561/s1, Table S1: RST Sample Locations and Notes; Table S2: SEM EDX data.

Author Contributions: Conceptualization, J.C. and J.B.; methodology, J.C., J.B. and R.H.; software, J.C. and R.H.; validation, J.C. and R.H.; formal analysis, J.C. and R.H.; investigation, J.C. and R.H.; resources, J.B. and R.H.; data curation, J.C.; writing—original draft preparation, J.C.; writing—review and editing, J.C., J.B. and R.H.; visualization, J.C.; supervision, J.C. and J.B.; project administration, J.C.; funding acquisition, J.C. and J.B. All authors have read and agreed to the published version of the manuscript.

Funding: This research was funded by graduate student research grants awarded to Julian Cohen by The Geological Society of the Oregon Country and The Central Oregon Geoscience Society.

Institutional Review Board Statement: Not applicable.

Informed Consent Statement: Not applicable.

Data Availability Statement: All data created as part of this work are openly available in the text or in supplemental tables published with this manuscript.

Acknowledgments: Thanks to Jeff Cullen at the University of Texas, Austin for his help with the isotope analyses presented in this work.

Conflicts of Interest: The authors declare no conflicts of interest.

References

1. Friedman, I.; Gleason, J.; Warden, A. Ancient Climate from Deuterium Content of Water in Volcanic Glass. *Clim. Chang. Cont. Isot. Rec. Am. Geophys. Union (AGU)* **1993**, *78*, 309–319. [CrossRef]
2. Cassel, E.J.; Graham, S.A.; Chamberlain, C.P. Cenozoic tectonic and topographic evolution of the northern Sierra Nevada, California, through stable isotope paleoaltimetry in volcanic glass. *Geology* **2009**, *37*, 547–550. [CrossRef]
3. Saylor, J.E.; Horton, B.K. Nonuniform surface uplift of the Andean plateau revealed by deuterium isotopes in Miocene volcanic glass from southern Peru. *Earth Planet. Sci. Lett.* **2014**, *387*, 120–131. [CrossRef]
4. Bershaw, J.; Cassel, E.J.; Carlson, T.B.; Streig, A.R.; Streck, M.J. Volcanic glass as a proxy for Cenozoic elevation and climate in the Cascade Mountains, Oregon, USA. *J. Volcanol. Geotherm. Res.* **2019**, *381*, 157–167. [CrossRef]
5. Sundell, K.E.; Saylor, J.E.; Lapen, T.J.; Horton, B.K. Implications of variable late Cenozoic surface uplift across the Peruvian central Andes. *Sci. Rep.* **2019**, *9*, 4877. [CrossRef]
6. Ross, C.S.; Smith, R.L. Water and other volatiles in volcanic glasses. *Am. Miner.* **1955**, *40*, 1071–1089.
7. Friedman, I.; Gleason, J.; Sheppard, R.A.; Gude, A.J., 3rd. Deuterium Fractionation as Water Diffuses into Silicic Volcanic Ash. *Clim. Chang. Cont. Isot. Rec. Am. Geophys. Union (AGU)* **1993**, *78*, 321–323. [CrossRef]
8. Cassel, E.J.; Breecker, D.O. Long-term stability of hydrogen isotope ratios in hydrated volcanic glass. *Geochim. Et Cosmocimica Acta* **2017**, *200*, 67–86. [CrossRef]
9. Wells Ray, E.; Snavely Parke, D. *Cenozoic Evolution of the Continental Margin of Oregon and Washington*; USGS Open-File Report Open-File Report; United States Geological Survey: Reston, VA, USA, 1991.
10. Retallack, G. Cenozoic Paleoclimate on Land in North America. *J. Geol.* **2007**, *115*, 271–294. [CrossRef]
11. McLean, A.; Bershaw, J. Molecules to Mountains: A Multi-Proxy Investigation into Ancient Climate and Topography of the Pacific Northwest, USA. *Front. Earth Sci.* **2021**, *9*, 624961. [CrossRef]
12. Priest, G.R. Volcanic and tectonic evolution of the Cascade Volcanic Arc, central Oregon. *J. Geophys. Res.* **1999**, *95*, 583–599. [CrossRef]
13. Kohn, M.J.; Miselis, J.L.; Fremd, T.J. Oxygen isotope evidence for progressive uplift of the Cascade Range, Oregon. *Earth Planet Sci. Lett.* **2002**, *204*, 151–165. [CrossRef]
14. Kukla, T.; Rugenstein, J.K.C.; Ibarra, D.E.; Winnick, M.J.; Stromberg, C.A.E.; Chamberlain, C.P. Drier Winters Drove Cenozoic Open Habitat Expansion in North America. *AGU Adv.* **2021**, *3*, e2021AV000566. [CrossRef]
15. Streck, M.J.; Grunder, A.L. Crystallization and welding variations in a widespread ignimbrite sheet; the Rattlesnake Tuff, eastern Oregon, USA. *Bull. Volcanol.* **1995**, *57*, 151–169. [CrossRef]
16. Streck, M.J.; Grunder, A.L. Temporal and crustal effects on differentiation of tholeiite to calcalkaline and ferro-trachytic suites, High Lava Plains, Oregon, USA. *Geochem. Geophys. Geosyst.* **2012**, *13*, Q0AN02. [CrossRef]
17. Streck, M.J. *Volcanology and Petrology of the Rattlesnake Ash-Flow Tuff*; Oregon State University: Corvallis, OR, USA, 1994; 199p, Available online: https://scholar.google.com/scholar_url?url=https://ir.library.oregonstate.edu/dspace/bitstream/1957/8357/1/Streck_Martin_J.pdf&hl=en&sa=X&ei=uv0AZLXpHY7gygSPuIegDA&scisig=AAGBfm3H7vSRTN-0S2T0R-fn9ynkadNnPA&oi=scholarr (accessed on 2 March 2023).
18. Freundt, A.; Wilson, C.J.N.; Carey, S.N. Ignimbrites and Block-and-Ash Flow Deposits. In *Encyclopedia of Volcanoes*; Academic Press: Cambridge, MA, USA, 1999; pp. 581–599.
19. Walker, G.W. Cenozoic Ash Flow Tuffs of Oregon. *Ore Bin* **1970**, *32*, 97–115.
20. Greene, R.C.; Walker, G.W.; Corcoran, R.E. *Geologic map of the Burns Quadrangle, Oregon*; US Geological Survey: Reston, VA, USA, 1972. Available online: https://ngmdb.usgs.gov/Prodesc/proddesc_9455.htm (accessed on 2 March 2023).

21. Caves, J.K.; Winnick, M.J.; Graham, S.A.; Sjostrom, D.J.; Mulch, A.; Chamberlain, C.P. Role of the westerlies in Central Asia climate over the Cenozoic. *Earth Planet. Sci. Lett.* **2015**, *428*, 33–43. [CrossRef]
22. Streck, M.; Grunder, A. Compositional Gradients and Gaps in High-silica Rhyolites of the Rattlesnake TuV. *J. Petrol.* **1997**, *38*, 133–163. [CrossRef]
23. Carlson, T. Volcanic Glass as a Paleoenvironmental Proxy: Comparing Preparation Methods on Ashes from the Lee of the Cascade Range in Oregon, USA. Master's Thesis, Portland State University, Portland, OR, USA, 2018. [CrossRef]
24. Bowen, G.J. Gridded Maps of the Isotopic Composition of Meteoric Waters. 2024. Available online: http://www.waterisotopes.org (accessed on 13 February 2024).
25. IAEA/WMO. Global Network of Isotopes in Precipitation. The GNIP Database. 2015. Available online: https://nucleus.iaea.org/wiser (accessed on 12 February 2024).
26. Welker, J.M. Isotopic (d18O) characteristics of weekly precipitation collected across the USA: An initial analysis with application to water source studies. *Hydrol. Process.* **2000**, *14*, 1449–1464. [CrossRef]
27. Bowen, G.J.; Revenaugh, J. Interpolating the isotopic composition of modern meteoric precipitation. *Water Resour. Res.* **2003**, *39*, 1299. [CrossRef]
28. Kotov, A.; Smirnov, S.; Plechov, P.; Persikov, E.; Chertkova, N.; Maksimovich, I.; Karmanov, N.; Bukhtiyarov, P. Method for Determining Water Content in Natural Rhyolitic Melts by Raman Spectroscopy and Electron Microprobe Analysis. *Petrology* **2021**, *29*, 386–403. [CrossRef]
29. Bershaw, J.; Penny, S.M.; Garzione, C.N. Stable isotopes of modern water across the Himalaya and east-ern Tibetan Plateau: Implications for estimates of paleoelevation and paleoclimate. *J. Geophys. Res.* **2012**, *117*. [CrossRef]
30. Seligman, A.N.; Bindeman, I.N.; Watkins, J.M.; Ross, A.M. Water in volcanic glass: From volcanic degassing to secondary hydration. *Geochim. Cosmochim. Acta* **2016**, *191*, 216–238. [CrossRef]
31. Befus, K.S.; Walowski, K.J.; Hervig, R.L.; Cullen, J.T. Hydrogen Isotope Composition of a Large Silicic Magma Reservoir Preserved in Quartz-Hosted Glass Inclusions of the Bishop Tuff Plinian Eruption. *Geochem. Geophys. Geosyst.* **2020**, *21*, e2020GC009358. [CrossRef]
32. Giachetti, T.; Gonnermann, H.M.; Gardner, J.E.; Shea, T.; Gouldstone, A. Discriminating secondary from magmatic water in rhyolitic matrix-glass of volcanic pyroclasts using thermogravimetric analysis. *Geochim. Cosmochim. Acta* **2015**, *148*, 457–476. [CrossRef]
33. Dansgaard, W. Stable isotopes in precipitation. *Tellus* **1964**, *16*, 436–468. [CrossRef]
34. Rozanski, K.; Araguás-Araguás, L.; Gonfiantini, R. Isotopic patterns in modern global precipitation. *Clim. Chang. Cont. Isot. Rec.* **1993**, *78*, 1–36.
35. Waterisotopes Database. Query: Country = US, Type = River or Stream, Precipitation. Available online: http://waterisotopesDB.org (accessed on 12 January 2022).
36. Greenwood, C.; Portland State University, Portland, OR, USA. Personal communication, 2024.
37. Brooks, J.R.; Wigington, P.J., Jr.; Phillips, D.L.; Comeleo, R.; Coulombe, R. Willamette River Basin surface water isoscape (δ18O and δ2H): Temporal changes of source water within the river. *Ecosphere* **2012**, *3*, art39. [CrossRef]
38. Poulsen, C.J.; Jeffery, M.L. Climate change imprinting on stable isotopic compositions of high-elevation meteoric water cloaks past surface elevations of major orogens. *Geology* **2011**, *39*, 595–598. [CrossRef]
39. Galewsky, J. Orographic precipitation isotopic ratios in stratified atmospheric flows: Implications for paleoelevation studies. *Geology* **2009**, *37*, 791–794. [CrossRef]
40. Tachera, D.K.; Lautze, N.C.; Torri, G.; Thomas, D.M. Characterization of the isotopic composition and bulk ion deposition of precipitation from Central to West Hawaii Island between 2017 and 2019. *J. Hydrol. Reg. Stud.* **2021**, *34*, 100786. [CrossRef]
41. Kukla, T.; Ibarra, D.E.; Rugenstein, J.K.C.; Gooley, J.T.; Mullins, C.E.; Kramer, S.; Moragne, D.Y.; Chamberlain, C.P. High-Resolution Stable Isotope Paleotopography of the John Day Region, Oregon, United States. *Front. Earth Sci.* **2021**, *9*, 30. [CrossRef]
42. Ford, M.T.; Grunder, A.L.; Duncan, R.A. Bimodal volcanism of the High Lava Plains and Northwestern Basin and Range of Oregon: Distribution and tectonic implications of age-progressive rhyolites. *Geochem. Geophys. Geosyst.* **2013**, *14*, 2836–2857. [CrossRef]
43. Jordan, B.T.; Grunder, A.L.; Duncan, R.A.; Deino, A.L. Geochronology of age-progressive volcanism of the Oregon High Lava Plains: Implications for the plume interpretation of Yellowstone. *J. Geophys. Res. Solid Earth* **2004**, *109*, B10202. [CrossRef]
44. Swenton, V.M.; Streck, M.J.; Miggins, D.P.; McIntosh, W.C. Filling critical gaps in the space-time record of High Lava Plains and co-Columbia River Basalt Group rhyolite volcanism. *GSA Bull.* **2022**, *135*, 1415–1428. [CrossRef]
45. Hildreth, W.; Fierstein, J. *The Novarupta-Katmai Eruption of 1912—Largest Eruption of the Twentieth Century: Centennial Perspectives*; Professional Paper; United States Geological Survey: Reston, VA, USA, 2012.
46. Carn, S.A.; Pallister, J.S.; Lara, L.; Ewert, J.W.; Watt, S.; Prata, A.J.; Thomas, R.J.; Villarosa, G. The Unexpected Awakening of Chaitén Volcano, Chile. *EOS Trans. Am. Geophys. Union* **2009**, *90*, 205–206. [CrossRef]